To Dr. Roussos, Topical Editor

The submitted manuscript has been substantially revised by including my answers in the interactive discussion, as well as significance of case study of Saka and Hayashi (2017). A new evidence of geosynchronous dipolarization is added in Appendix.

Each issue has been addressed in the prescribed Comment/Response format. These responses were marked in the manuscript in bold and were specified by line numbers.

Point-by-point replies to the comments raised by Referee #1 is given below.

Comment:
The author proposes a new idea on the cause of magnetospheric substorms. He proposes that the fast plasma flows from the magnetotail changes the curvature of magnetic field lines at the geosynchronous distance. This produces an electric field which can generate Bostrom's current system. I did not follow every detail of his mathematical analysis, but it seems reasonable. If the author has a chance to revise the paper, he might discuss the relationship between the fast plasma flows and the occurrence of magnetospheric substorms.

Response:
The role of fast earthward flows in our substorm onset scenario is briefly described.

We first assumed that the geosynchronous altitudes are earthward end of the flow penetration of fast earthward flows from the magnetotail. Because field lines passing through the geosynchronous altitudes stretched tailward at the substorm onset, the initial brightening of auroras triggered by the fast flows may occur, statistically, at lower latitudes, 63 degrees N in geomagnetic coordinates for Kp=4 [Saka, 2019]. This may be the most equatorward latitude of the breakups.

Secondly, we note that substorm onset is a transitional state lasting for several Pi2 cycles (10 min) after the Pi2 onset followed by formation of the substorm current wedge by reduction of cross-tail currents. We can assume that dipolarization fronts (DFs) arrive in the transitional interval and the flow braking may occur afterwards in association with the

reduction of cross-tail currents, viz., subsequent formation of the substorm current wedge. Of course, this scenario was deduced from the geosynchronous observation and cannot be readily applied to the onset scenario beyond the geosynchronous orbit. Nevertheless, if dawn-dusk expansion of the flux tubes in our scenario caused by the Ballooning instability (excites slow magnetoacoustic wave) is applicable to the formation of dipolarizing flux bundles (DFBs) propagating earthward within fast earthward flows (BBFs) [Liu et al., 2015], the results from geosynchronous observations we presented can be extended further tailward in upstream. Or, the onset scenario in 8 -12 Re can be applied in geosynchronous dipolarization.
Lines 276-293.

Point-by-point replies to the comments raised by Referee #2 is given below.

Comment:
The author proposed an interesting hypothesis to assemble terrestrial magnetic dipolarization, initiated from the geosynchronous altitudes. To the referee's understanding, what drivers magnetic dipolarization is very complicated, so far there have been many proposed scenarios in driving dipolarization process. After numerous measurements in Earth's magnetosphere, it is generally believed that many fundamental processes are involved in driving magnetic dipolarization. The proposed mechanism in this paper is likely over simplified. It looks too speculative to the referee, especially there is no any support from in situ observations. Therefore the referee could not recommend this paper for a publication. However, if the hypothesis could be supported by some case study, it would make much more sense and shall have potential for a publication.

Response:
As far as the onset is concerned, poor timing accuracy may obscure the substorm study. In statistical analyses presented in Saka et al (2010), we used initial peak of Pi2 amplitudes as a timing reference. This gave the timing accuracy less than 1 minute for the onset study. As a result, we could sort out fundamental processes of substorm associated with the onset, such as transitional interval preceding the field line pileup. It was also found that field lines in the transitional intervals expanded in dawn-dusk directions and decreased field magnitudes therein. We presented case study of geosynchronous onset of field line dipolarization from Saka and Hayashi (2017). This event demonstrated that equatorward inflows that produced parallel flows along the field lines eventually triggered the dipolarization onset (slow

magnetoacoustic wave) and it deflected the flow directions to dawn-dusk (perpendicular to the field lines). We suggest that, on the statistical bases as well as for case study, longitudinal expansion in both plasma flows and field lines is a fundamental process associated with the dipolarization onset. The aim of this paper is to propose a driver model of the longitudinal expansion.

Comment 1:

Why ballooning instability could develop in geosynchronous orbit? Comparison between the scale of pressure gradient and curvature radius is necessary.

Response:

We used calculation results of Ballooning instability given in [Rubtsov et al., 2018]. In a distance from L=5 to 10Re, instability threshold is given approximately as $\kappa = -1.0\,\mathrm{Re}^{-1}$ (κ denotes reciprocal spatial scale of radial inhomogeneity of plasma pressure) for beta defined by the ratio of plasma pressure and magnetic pressure exceeding 0.1. This suggests that the Ballooning instability develops at the geosynchronous altitudes (curvature radius R is 2.2 Re) when spatial scale of the earthward pressure gradient caused by the inflows becomes steeper than 1.0 Re. This result matched observation (see Appendix).

Lines 143-150.

Comment 2:

Substorm onset is usually believed triggered at _10 Re, and the auroral beads which manifest ballooning instability is also believed to map to _10 Re but not at geosynchronous orbit. The geosynchronous orbit initiation of dipolarization is not supported by observations.

Response:

Inflows of lobe plasma [Birn and Hesse, 1996], Poynting flux [Machida et al., 2009], and Ey penetration [Machia et al., 2014] towards the equatorial plane may be a primary driver of substorms. If enough inflows, Poynting flux, and Ey penetration occurred at geosynchronous altitudes, dipolarization initiate there. We presented example of the geosynchronous dipolarization event in Appendix.

Lines 310-340.

Comment 3:

Why the hypothesis must be applied in geosynchronous but not 10Re? The magnetic stretching process is also clearly shown in 10Re region, for example, the substorm event shown in Sergeev et al. 2011, doi:10.1029/2010JA015689.

Response:

The proposed scenario was deduced from the geosynchronous observation and cannot be readily applied to the onset scenario beyond the geosynchronous orbit. Nevertheless, dawn-dusk expansion of the flux tubes may be a fundamental property of field line dipolarization not only at geosynchronous altitudes but also in tailward locations (8 -12 Re) [Yao et al., 3013; Liu et al., 2013]. It is suggested that the field line dipolarization at tailward locations is subdivided into faster expanding (in longitudes) dipolarization front (DF) and slower expanding dipolarization front bundle (DFB) led by DF [Liu et al., 2015]. Such substructures in field line dipolarization are also observed at geosynchronous altitudes [Saka and Hayashi, 2017]. The geosynchronous dipolarization expanded (in longitudes) at 1.9 km/s, while Pi2s emitted in the dipolarization region propagated one order of magnitude faster. The fast longitudinal velocities associated with Pi2s may be embedded within the slowly expanding region of dipolarization, similarly to the relationship between DF and DFB. If this relationship can be adapted also to transitional state and succeeding field line pileup, the dipolarization scenario from geosynchronous observations can be extended further tailward in upstream. Or, the onset scenario in 10 Re can be applied in geosynchronous dipolarization. In that case, dipolarization pulse at Goes6 latitudes ($7.9^{\circ}N$) may represents DFs.

Lines 276-293.

Comment 4:

The dawn dusk stretching flux tube is a common feature ahead of dipolarization front, (e.g., Figure 4 in Yao et al. 2013 doi:10.1002/2013JA019290 and Figure 6 in Liu et al. 2013 doi:10.1002/jgra.50092).

Response:

The above references were added to the revised version.

Line 280.

Comment 5:

It has been reported that BBFs decelerate dramatically when they propagate towards the Earth [Shiokawa et al., 1997]. And It could be hardly for DFs arrival at geosynchromous.

Thus, the hypothesis that westward electric fields on DFs trigger instability at geosynchromous should be not universal. The author needs to discuss in which conditions the proposed scenarios could be applied.

Response:

We proposed that substorm onset is a transitional state lasting 10 min after the Pi2 onset followed by formation of the substorm current wedge by reduction of cross-tail currents. We can assume that DFs arrive in the transitional interval and the flow braking may occur afterwards in association with the reduction of cross-tail currents, viz., subsequent formation of the substorm current wedge. It is likely that the flow braking does not affect the arrival of DFs.

Comment 6:

line 100: It requires more explanation for Eq. 1:

Response:

At geosynchronous altitudes, field line stretching started 90 minutes prior to the substorm onset [Figure 1 of Saka, 2019]. The stretching decreased the field line inclination by 7 degrees from 40.6 to 33.6 in this 90-min interval. This gives angular velocity of rotation of field line inclination in Equation (1) as $1.4\times10^{-3}\ rad/\min$. Total parallel flux gained in T min may be given by the integral of equation (1) with time from 0 to T. Substituting T=60 min and $1.4\times10^{-3}\ rad/\min$ for angular velocity of field line inclination, this yields $F_{//}=8.2\times10^{-2}\cdot F_{\perp}$. Gain of $F_{//}$ is about 10% of the perpendicular flux ($F_{\perp}$). This is consistent with the parallel temperature anisotropies (20% gain) observed at geosynchronous orbit [Birn et al., 1997].

Lines 91-116.

Comment 7:

line 258-262: it is unclear why the change of curvature radius of field lines is different from the flux pileup dipolarization. Both are caused by current disruption, can we distinguish between them in observations?:

Response:

Changes of curvature radius occurred in the geosynchronous orbit in association with

longitudinal expansion of flux tubes which decreased field magnitudes therein. It lasted about 10 minutes after the Pi2 onset. The change of curvature radius is thought to be caused by the transition of the flux tubes to a new equilibrium configuration. This is often observed in the initial pulse of Pi2s as third harmonic deformation of field lines [Saka et al., 2012]. Of course, cross-tail currents decrease according to Ampere's law. The flux pileup characterized by the increase of the field magnitudes at geosynchronous altitudes began after this 10-min interval. This post 10-min-interval is organized by reduction in cross-tail currents (formation of the substorm current wedge) which were deduced from the field line observations by Goes 5 and Goes 6 satellites at different latitudes from the equatorial plane. Please refer to [Saka et al., 2010].

The increase of curvature radius of geomagnetic field lines preceding a classical dipolarization

Osuke Saka
Office Geophysik, Ogoori, 838-0141, Japan

Abstract

We discuss substorm field line dipolarization at geosynchronous altitudes associated with high velocity magnetotail flow bursts referred to as Bursty Bulk Flows. In growth phase, we found that the magnetosphere at geosynchronous orbit are in unstable conditions for Ballooning instability due to the appreciable tailward stretching of the flux tubes, and for slow magnetoacoustic wave due to the continuing field-aligned inflows of plasma sheet plasmas towards the equatorial plane. We propose following scenario of field line dipolarization; (1) The slow wave was excited through Ballooning instability by enhanced inflows towards the equatorial plane. (2) In the equatorial plane, slow wave stretched the flux tube in dawn-dusk directions, which resulted in the spreading plasmas in dawn-dusk directions and reducing the radial pressure gradient in the flux tube. (3) As a result, the flux tube becomes a new equilibrium geometry in which curvature radius of new field lines increased in meridian plane, suggesting an onset of field line dipolarization. The dipolarization processes associated with changing the curvature radius preceded classical dipolarization caused by reduction of cross-tail currents and pileup of the magnetic fields.

Increasing curvature radius induced inductive electric fields of the order of few mV/m pointing westward in the equatorial plane, as well as radial electric fields associated with stretching flux tubes in dawn-dusk directions. Westward electric fields transmitted to the ionosphere produce a dynamic ionosphere where the E layer contains both dynamo ($\mathbf{E}\cdot\mathbf{J}<0$) and dissipation ($\mathbf{E}\cdot\mathbf{J}>0$) processes in it for generating field-aligned current system of Bostrom type.

1. Introduction

Substorms are spatially localized and temporarily variable processes in the nighttime magnetosphere. It is often difficult to determine onset timing of substorm processes such as magnetotail flow burst, field line dipolarization, and particle injections. To resolve the timing uncertainties, auroras in global satellite images [Nakamura et al., 2001; Miyashita et al.,

2009], intensifications of auroral kilometric radiation [Fairfield et al., 1999; Morioka et al., 2010], and dispersionless particle injection in geosynchronous orbit [Birn et al., 1997] were used. Ground Pi2 pulsations are another useful tool for determination of the substorm timing [Sakurai and Saito, 1976; Nagai et al., 1998; Baumjohann et al., 1999]. Particularly, Pi2s in equatorial region exhibited small phase difference (m<1, m denotes azimuthal wave number) across widely separated stations in the equatorial countries [Kitamura et al., 1988]. This enabled us accurate onset timing study of substorms using magnetometer data from two remote locations, geosynchronous altitudes and conjugate ground stations of the equatorial countries [Saka et al., 2010].

In this study, we focus on the dipolarization events at geosynchronous orbit from growth to expansion phase. Triggering mechanisms of the field line dipolarization in the vicinity of geosynchronous orbit are our major concern. We apply geosynchronous scenario to tailward dipolarization. In this paper, onset timing study of substorms using magnetometer data from equatorial countries are summarized in Sect. 2. In Sect. 3, we present a pre-onset scenario leading to the dipolarization onset. We will focus on the field line dipolarization in the vicinity of geosynchronous orbit in Sect. 4. A coupling of magnetosphere and ionosphere associated with this dipolarization scenario will be presented in Sect. 5. Summary and discussion of this scenario is given in Sect. 6. In Appendix, observational evidence of the instability threshold of dipolarization onset is presented.

2. Summary of onset timing study using ground Pi2s at the equator

In this section, we summarize field line dipolarization occurring at the geosynchronous orbit based on the statistical results obtained by Saka et al. [2010]. The authors used magnetometer data from geosynchronous satellites (Goes5 and Goes6) and those at ground equatorial stations (Huancayo, Peru) in the conjugate meridian. Goes5 was located at higher latitudes, $10.3^{\circ}N$ in dipole coordinates, and Goes6 was closer to the equator; $7.9^{\circ}N$ in dipole coordinates. This difference was caused by the separated meridians of the satellites (285° for Goes5, 252° for Goes6). The dipole coordinate used are equivalent to the HDV coordinates; H is positive northward along the dipole axis, V is radial outward, and D denotes dipole east. The field line dipolarization at the geosynchronous orbit can be characterized either by a step-like or impulsive increase of inclination angle of the geomagnetic field lines. The inclination angle is measured positive northward from the dipole equator. The step-like dipolarization was observed by Goes5 located at higher latitudes, while the dipolarization pulse was observed by Goes6 at latitudes closer to the equatorial plane.

The onset of field line dipolarization preceded the initial peak of the ground Pi2 pulse by two

minutes, suggesting that the onset was initiated in association with the first increase of the Pi2 amplitudes. Following the dipolarization onset, field line magnitude decreased at the geosynchronous orbit, and field lines deflected westward (eastward) in the dawn (dusk) sector. The authors suggested that field line deflections decreased the field magnitudes therein by the longitudinal expansion of flux tubes. Decrease of field magnitudes and westward deflections of field lines lasted for several Pi2 cycles (10 min). Eastward deflections in the dusk sector, however, continued over this characteristic 10-min-interval. After this 10-min-interval, Pi2 amplitudes weakened and field magnitudes turned to increase. It is suggested that classical dipolarization, caused by the reduction of cross-tail currents in the midnight magnetosphere, happened after the nightside magnetosphere experienced this characteristic 10-min-interval. For this reason, the first 10 min intervals are referred to as transitional state of substorm expansion [Saka et al., 2010].

3. Pre-onset intervals leading to field line dipolarization

In the pre-onset intervals, decrease of the field line inclination started two hours prior to the dipolarization onset. It attained minimum angles (33.6^{o} for Goes5 and 49.4^{o} for Goes6 in dipole coordinates) right before the dipolarization onset [Saka, 2010; 2019].

One of the properties of plasmas in pre-onset intervals are continuing inflows of lobe plasmas towards the equatorial plane [Birn and Hesse, 1996], Poynting flux enhancement [Machida et al., 2009], and Ey penetration toward the equatorial plane [Machida et al, 2014]. Corresponding plasma properties at geosynchronous altitudes may be predominant perpendicular temperature anisotropies of thermal plasmas (30eV - 40keV) and their gradual decrease towards the onset [Birn et al., 1997]. At the onset, however, increase of parallel anisotropy stopped and perpendicular anisotropy increased again. This transition of the temperature anisotropy may be accounted for by the following manner. A continuing tailward stretch of the field lines in the pre-onset intervals as depicted in Figure 1 may increase equatorward flux by the counterclockwise rotation of the inflow ($F_{\perp}$) vectors and produce parallel component as well by the relation,

$$\delta F_{//} = F_{\perp}(\omega \cdot \delta t) \qquad \textbf{(1)}$$

Here, $\delta F_{//}$ denotes increase of parallel flux per time, δt, ω is angular velocity of counterclockwise rotation of $F_{\perp}$ vectors associated with the thinning of the flux

tubes caused by stretching. In pre-onset intervals lasting 90 min at geosynchronous altitudes, field line stretching decreased the field line inclination by 7° from 40.6° to 33.6° (see Figure 1 in [Saka, 2019]). This gives angular velocity of rotation of field line inclination in equation (1) as $1.4\times10^{-3}\ rad/\min$. Total parallel flux gained in T min may be given by the integral of equation (1) with time from 0 to T. Substituting T=60 min and $1.4\times10^{-3}\ rad/\min$ for angular velocity of field line inclination, this yields $F_{//}=8.2\times10^{-2}\cdot F_{\perp}$. Gain of $F_{//}$ is about 10% of the perpendicular flux ($F_{\perp}$). This is consistent with the parallel temperature anisotropies gained prior to the onset (20% gain) in geosynchronous orbit [Birn et al., 1997]. Increasing equatorward component of inflows are also reported as characteristic property of thermal plasmas in the pre-onset intervals at geosynchronous altitudes [Saka and Hayashi, 2017].

Continuing parallel flux flows associated with the flux tube thinning in the pre-onset intervals may increase plasma pressures in the flux tube at its tailward end. This condition leads to further stretching of the flux tube (small curvature radius) [Ohtani and Tamao, 1993; Rubtsov et al., 2018] by the relation,

$$\frac{\beta}{2}\kappa+\kappa_B+\frac{1}{R}=0 \qquad (2)$$

Here, β is plasma to magnetic pressure ratio, κ and κ_B denote reciprocal spatial scales of radial inhomogeneity of plasma pressure and magnetic fields in the equatorial plane, respectively. R is curvature radius of the field lines. A further increase of κ associated with more steeper pressure gradient in earthward direction may trigger Ballooning instability [Rubtsov et al., 2018].

An increase of parallel flux may also lead to the unstable condition for slow magnetoacoustic wave. After manipulating a set of linearized MHD equations of magnetoacoustic waves [Kadomtsev, 1976], we have a relation between parallel displacement along the field lines (ξ_z) and perpendicular stretching of the field lines ($\xi_{\perp}$) in the following form,

$$\xi_z=\frac{C_S^2}{\omega^2}F\cdot B_0^2\frac{\partial}{\partial z}(div\xi_{\perp}) \qquad (3)$$

Here, C_s, ω and B_0 are the sound velocity, angular frequency of waves and background field magnitudes, respectively. *F* is given by

$$F = \frac{C_A^2}{B_0^2} \frac{1}{C_s^2 - (\frac{\omega}{k})^2} \qquad (4)$$

F is positive for the slow magnetoacoustic wave and negative for the fast magnetoacoustic wave. C_A denotes Alfven velocity. If the wave mode was the fast mode, flux tubes would have contracted in longitudes towards the midnight sector, which was not observed during the transitional state of substorm expansion (see Section 2).

It is therefore expected in the pre-onset intervals that slow magnetoacoustic wave coupled with Alfven wave are in unstable conditions. These waves can be excited by the Ballooning instability [Ohtani and Tamao,1989; Rubtsov et al., 2018], if κ in equation (2) exceeds a threshold.

We can estimate the Ballooning instability threshold κ using calculation results given in [Rubtsov et al., 2018]. In a distance from L=5 to 10Re, instability threshold is given approximately as $\kappa = -1.0\,\mathrm{Re}^{-1}$ (κ denotes reciprocal spatial scale of radial inhomogeneity of plasma pressure, and Re is the Earth radius) for beta defined by the ratio of plasma pressure and magnetic pressure exceeding 0.1. This suggests that the Ballooning instability develops at the geosynchronous altitudes (curvature radius R is 2.2 Re) when spatial scale of the earthward pressure gradient caused by the inflows becomes steeper than 1.0 Re. This result matched observation (see Appendix).

4. Field line dipolarization in the vicinity of geosynchronous orbit

We can assume the westward electric fields in Dipolarization Front (DF) [Runov et a., 2011] embedded in the leading edge of Bursty Bulk Flow (BBF) as external stimulus for triggering Ballooning instability. In this case westward electric fields in the DF temporarily amplified the parallel flux flowing towards the end point of the flux tube in the equatorial plane and further steepen earthward pressure gradient. If it exceeds instability threshold determined by β and initial curvature radius *R*, slow magnetoacoustic wave can be excited [Rubtsov et al., 2018]. Once the slow magnetoacoustic wave was excited, stretched flux tubes in the equatorial pane as depicted in Figure 2 spread the plasmas in dawn-dusk directions and smooth (or relax) the radial gradient of plasma pressures in the equatorial plane (smaller κ). This may result in the transition of the flux tube geometry to a new configuration, an increase of the curvature radius of the field lines (larger *R*) (see equation (2)).

Meanwhile, field lines in the further earthward locations may be compressed by the inward movement of the outer field lines. This process associated with the dipolarization onset may increase the parameter κ_B in equation (2) which may result in transition to a new geometry

of earthward field lines, a decrease of the curvature radius *R*. Transition of the field line geometries for onset locations and ones in earthward locations are schematically illustrated in Figure 3. These field line geometries matched the third harmonic and fundamental harmonic deformations of outer and inner field lines, respectively. This is often observed in the midnight magnetosphere in the initial pulse of Pi2s [Saka et al., 2012]. Transitions of the flux tube geometry in magnetosphere also correspond to the production of negative bay in higher latitudes and positive bay in lower latitudes. If we can assume that negative bay switched to positive bay at latitudes, 60 degrees in geomagnetic coordinates for examples, this latitude can be mapped beyond the geosynchronous orbit (L~7 Re or further tailward) as field line dipolarization occurs along the stretched flux tubes. Consequently, this scenario requires that the BBFs are not necessary to reach inner magnetosphere to trigger the substorm onset at lower latitudes.

Increasing of the curvature radius, or earthward shrinkage of the flux tubes, produce a reduction of the radial component of the field lines (V in dipole coordinates) by adding positive V in the north of the equatorial plane and negative V in the south. If amplitudes of the V component changed by 10 nT in one minute, the expected inductive electric fields (westward) could be of the order of 1.0 mV/m when shrinkage was confined within 1 Re from the equatorial plane. The dawn-dusk expansion of the flux tubes may also produce inductive electric fields (earthward and tailward in dawn and dusk sector, respectively) of the same order of magnitudes. The westward electric fields produce earthward flow bursts referred to as convection surge. The inductive electric fields produced by the dipolarization are the same order of magnitudes observed in DF [Runov et al., 2011].

5. Coupling of magnetosphere and ionosphere in association with field line dipolarization

The inductive electric fields may be transmitted along the field lines as poloidally and toroidally polarized Alfven waves [Klimushkin et al., 2004]. These electric fields produce a dynamic ionosphere in polar region that includes nonlinear evolution of ionospheric plasmas (poleward expansion), as well as production of field-aligned currents and parallel potentials by exciting ion acoustic wave in quasi-neutral condition [Saka, 2019]. It is not the aim of this paper to describe in detail the dynamic processes in the ionosphere, but to show a local production of currents in the ionosphere as well as field-aligned currents by the penetrated electric fields. For this purpose, we revisit the 10 August 1994 substorm event studied by Saka and Hayashi (2017). In this event, eastward expansion was observed of the field line dipolarization region. At the leading edge of the expansion, ground magnetometer data

showed bipolar event (quick change of the D component from positive to negative in about 5 min), being confined in the expanding dipolarization front as a substructure. The substructure in the leading edge of the field line dipolarization will be examined as follows.

We can assume that magnetic signals on the ground are associated with the sum of the horizontal Hall currents in the ionosphere [Fukushima, 1971]. These currents can be calculated by the relation,

$$(rot\,\mathbf{J})_Z = -\frac{1}{\mu_0}\nabla^2 B_Z \qquad (5)$$

We used the ground vertical component (*b*) as a proxy of B_z in the ionosphere. The second derivative in right-hand side of equation (5) is approximated as,

$$\nabla^2 B_Z^i = \left(\frac{b^{i+1}-b^i}{L_{i+1}-L_i} - \frac{b^i - b^{i-1}}{L_i - L_{i-1}}\right) / (L_{i+1} - L_{i-1}) \qquad (6)$$

Here, i denotes i-th station in the meridian chain. L_i is the geomagnetic latitude of the i-th station. We considered meridional change only. This is because the vertical component changed from negative to positive across the meridian, while in longitudes it changed simply decreasing or increasing in lower and higher latitudes after onset, respectively. The results reproduced from Saka and Hayashi (2017) are shown in Figure 4(A). The dipolarization front crossed this meridian at 12:13 UT corresponding to the interval labelled 1. Two points arose from this figure; (1) Hall current pair existed, CCW in the lower latitudes and CW in the higher latitudes, (2) These current patterns expand poleward. Current patterns in the interval from 1 to 5 in Figure 4(A) are illustrated in Figure 4(B) to facilitate the poleward expansion. It is clearly demonstrated that current pair forming CW in higher latitudes and CCW in lower latitudes expanded in time towards the pole. Bipolar change can be recorded in the D component data (not shown) when the ground station, FSIM in this case, passes from segment 1 to 2 in Figure 5(B). As a result, dipolarization front expanded eastward progressively by producing the poleward expansion at each meridian. The front left behind the current pattern comprising upward field-aligned currents in lower latitudes and downward in higher latitudes, or Bostrom type current system. We propose that the ionosphere itself has inherent dynamo in the E layer to drive this Bostrom type current system. The reasons are as follows;

In the E region, drift trajectories may be written [Kelley, 1989] for electrons by,

$$\mathbf{U}_{e\perp} = \frac{1}{B}[\mathbf{E}\times\hat{\mathbf{B}}] \qquad (7)$$

and for ions by,

$$\mathbf{U}_{i\perp} = b_i[\mathbf{E} + \kappa_i \mathbf{E}\times\hat{\mathbf{B}}]\,. \qquad (8)$$

Here, b_i is mobility of ions defined as $\Omega_i/(B\nu_{in})$, κ_i is defined as Ω_i/ν_{in}. Symbols Ω_i and ν_{in} are ion gyrofrequency and ion-neutral collision frequency, respectively. $\hat{\mathbf{B}}$ denotes a unit vector of the magnetic fields B. We assumed that $\mathbf{E}\times\mathbf{B}$ drifts for electrons and ions were driven by westward electric fields transmitted from the convection surge. Because of very low mobility of ions in E layer ($\kappa_i = 0.1$), electric field drifts accumulate electrons (not ions) in lower latitudes and produce stronger secondary southward electric fields in the ionosphere. The southward electric fields produced southward motion of ions due to the first term of equation (8). They carry Pedersen currents (ion currents) for producing quasi-neutrality of ionosphere. $\mathbf{E}_W\times\mathbf{B}$ drifts caused by the transmitted westward electric fields ($\mathbf{E}_W$) may propel electrons against southward electric fields from higher latitudes to lower latitudes ($\mathbf{E}_S\cdot\mathbf{J}<0$, dynamo) to maintain the potential drop for driving Pedersen currents ($\mathbf{E}_S\cdot\mathbf{J}>0$, dissipation). This means the ionospheric E layer contains both dynamo (E layer dynamo) and dissipation processes in it. In quasi-neutral condition, a small imbalance of particle densities of electrons and ions ($n_e - n_i \sim 10^2 m^{-3}$) may induce in lower latitudes negative potential region of the order of -100 kV with horizontal scale length of 100 km. To sustain this negative potential, upward field-aligned currents of the order of $1.0\mu A/m^2$ for $\Sigma_P \sim 10^0 S$ must flow. Downward field-aligned currents from the positive potential regions in the higher latitudes may also be expected. It is supposed that upward field-aligned currents may be composed of ions and downward currents are electrons to require stable equatorward ion flows in the Pedersen channel. Those field-aligned currents closing via Pedersen currents in the ionosphere and polarization currents in the magnetosphere comprised meridional current system of Bostrom type, or incomplete Cowling channel [Baumjohann, 1983]. They were driven by the E layer dynamo.

6. Discussion and Summary

Definition of field line dipolarization is a configuration change from stretching to shrinkage of geomagnetic field lines in the midnight meridian of magnetosphere. Two models have been proposed to account for the configuration change; diversion of the cross-tail currents via ionosphere, referred to as substorm current wedge (SCW), as first proposed in McPherron et al. [1973] and extinction of the cross-tail currents by a local kinetic instability, current disruption (CD) [Lui, 1996]. These models have been adopted for many decades to account for the critical issues associated with substorm onset. We propose, based on Ballooning instability scenario, that field line dipolarization is caused by the slow magnetoacoustic wave in which a small curvature radius of the stretched field lines in pre-onset intervals increased to larger curvature radius by spreading plasmas in the equatorial plane towards dawn-dusk directions. Dipolarization regions expand in longitudes and decrease field magnitudes by expanding flux tubes therein. This condition continued for several Pi2 cycles (about 10 min) and classical dipolarization caused by the reduction of cross-tail currents or pileup of the magnetic flux transported from the tail begins.

The proposed scenario was deduced from the geosynchronous observation and cannot be readily applied to the onset scenario beyond the geosynchronous orbit. Nevertheless, dawn-dusk expansion of the flux tubes may be a fundamental property of field line dipolarization not only at geosynchronous altitudes but also in tailward locations (8 - 12 Re) [Yao et al., 3013; Liu et al., 2013]. It is suggested that the field line dipolarization at tailward locations is subdivided by faster expanding (in longitudes) dipolarization front (DF) and slower expanding dipolarization front bundle (DFB) led by DF [Liu et al., 2015]. Such substructures in field line dipolarization are also observed at geosynchronous altitudes [Saka and Hayashi, 2017]. The geosynchronous dipolarization expanded (in longitudes) at 1.9 km/s, while Pi2s emitted in the dipolarization region propagated one order of magnitude faster. The fast longitudinal velocities associated with Pi2s may be embedded within the slowly expanding region of dipolarization, similarly to the relationship between DF and DFB. If this relationship can be adapted also to the transitional state and succeeding field line pileup, the dipolarization scenario from geosynchronous observations can be extended further tailward in upstream. Or, the onset scenario in 10 Re can be applied in geosynchronous dipolarization. In that case, dipolarization pulse at Goes6 latitudes ($7.9^{\circ}N$ **) may represents DFs.**

We emphasize that two different types of the dipolarization exist in the substorms; one is associated with change of curvature radius of field lines in the transitional state (faster expansion in longitudes) and the other is subsequent pileup of the magnetic flux transported from the tail (slower expansion). Tailward regression of the dipolarization region as reported

in Baumjohann et al. [1999] may be associated with the latter case.

In the transitional state lasting for about 10 min, the inductive electric fields pointing westward were produced in the equatorial plane. They propagated along the field lines to the ionosphere to produce dynamic ionosphere in the polar regions. The dynamic ionosphere has inherent dynamo processes in E layer producing meridional field-aligned currents of the Bostrom type (downward in higher latitudes and upward in lower latitudes). We found that Bostrom type current system was indeed observed on the ground at the front of dipolarization expanding towards east. The magnetospheric dynamo produced by earthward electric fields in the equatorial plane [Akasofu, 2003] and the E layer dynamo in the ionosphere worked together to activate the Bostrom current system.

7. Appendix

We checked the Ballooning instability threshold κ from satellite observations by revisiting multiple Pi2 events observed by AMPTE CCE on 31 August 1986 [Saka et al., 2002]. Results from [Saka et al., 2002] are reproduced in Figure 5. The satellite passed the midnight sector (20 – 23 MLT) from 3 Re to 7 Re at latitudes south of the equatorial plane (-8° MLat) when multiple Pi2 event (with positive bay) was observed at low latitude station (KUJ) at L=1.2 in the midnight sector (Figure 5C). At satellite altitudes, ion fluxes coming from dawn sector ($\mathbf{J}_{-}$) and from dusk sector ($\mathbf{J}_{+}$) were measured by the instruments (two energy channels, 63-85 keV and 125-210 keV) on board AMPTE CCE [Takahashi et al., 1996]. The flux difference ($\mathbf{J}_{-} - \mathbf{J}_{+} > 0$) suddenly increased in association with the onset of multiple Pi2 and positive bay at KUJ (Figures 5A and 5B). Sudden increase was followed by the slow decrease of flux in 63-85 keV channel and rapid decrease of flux in 125-210 keV channel. The flux difference, $\mathbf{J}_{-} > \mathbf{J}_{+}$, may be caused either by earthward pressure gradient or westward convection of plasmas. From the different patterns of the flux decrease with time in two energy channels, we can suggest that the measured flux difference, $\mathbf{J}_{-} - \mathbf{J}_{+}$, can be attributed to the sudden increase of the earthward pressure gradient and succeeding relaxation. The different relaxation speed in two energy channels, slower for 63-85 keV and faster for 125-210 keV, suggest that the pressure gradient (assumed to be proportional to the flux gradient) decreased with time during the multiple Pi2 event (see inset in Figure 5).

The flux difference (50 counts/sample) was 10% of the background flux both for 63-85 keV (Larmor radius is 250 km for 150 nT) and for 125-210 keV (Larmor radius is 450 km), that is, the flux level differed by 10% at two locations 1000 km (63-85 keV) and 1800 km (125-210 keV) apart in radial distance. This gives e-folding scale of the earthward pressure gradient being 0.98 Re and 1.77 Re for 63-85 keV and 125-210 keV, respectively. The 31 August event shows that radial pressure gradient was relaxed in the inner magnetosphere in association with the multiple Pi2 onset (positive bay in lower latitudes and negative bay in higher latitudes). We conclude that the relaxation of spatial inhomogeneity started when the spatial scale of the radial inhomogeneity approached 1.0 Re. This result supports Ballooning instability scenario of Rubtsov et al (2018) for the onset of field line dipolarization.

8. Code/Data availability

No data sets were used in this article.

9. Competing interest

The author declares that there is no conflict of interest.

Acknowledgements

The author would like to express his sincere thanks to all the members of Global Aurora Dynamics Campaign (GADC) [Oguti et al., 1988].

References

Akasofu, S.-I.: Source of auroral electrons and the magnetospheric substorm current system, J. Geophys. Res., 108, A4, 8006, doi:10.1029/2002JA009547, 2003.

Baumjohann, W.: Ionospheric and field-aligned current systems in the auroral zone: A concise review, Adv. Space Res., 2, 55-62, 1983.

Baumjohann, W., Hesse, M., Kokubun, S., Mukai, T., Nagai, T., and Petrukovich, A.A.: Substorm dipolarization and recovery, J. Geophys. Res., 104, 24995-25000, 1999.

Birn, J., Thomsen, M.F., Borovsky, J.E., Reeves, G.D., McComas, D.J., and Belian, R.D.: Characteristic plasma properties during dispersionless substorm injections at geosynchronous orbit, J. Geophys. Res., 102, A2, 2309-2324, 1997.

Fairfield, D.H., Mukai, T., Brittnacher, M., Reeves, G.D., Kokubun, S., Parks, G.K., Nagai, T.,

366 Mtsumoto, H., Hashimoto, K., Gurnett, D.A., and Yamamoto, T.: Earthward flow bursts
367 in the inner magnetotail and their relation to auroral brightenings, AKR intensifications,
368 geosynchronous particle injections and magnetic activity, J. Geophys. Res., 104, A1,
369 355-370, 1999.
370 Fukushima, N.: Electric current systems for polar substorms and their magnetic effect below
371 and above the ionosphere, Radio Sciences, 6, 269-275, 1971.
372 Kadomtsev, B.B.: Collective phenomena in plasmas (in Japanese), Iwanami shoten, Tokyo,
373 1976.
374 Kelley, M.C.: The earth's ionosphere: plasma physics and electrodynamics, Academic Press,
375 Inc, 1989.
376 Kitamura, T., Saka, O., Shimoizumu, M., Tachihara, H., Oguti, T., Araki, T., Sato, N., Ishitsuka,
377 M., Veliz, O., and Nyobe, J.B.: Global mode of Pi2 waves in the equatorial region:
378 Difference of Pi2 mode between high and equatorial latitudes, J. Geomag. Geoelectr,
379 40, 621-634, 1988.
380 Klimushkin, D.Yu., Mager, P.N., and Glassmeier, K.-H.: Toroidal and Poloidal Alfven waves
381 with arbitrary azimuthal wave numbers in a finite pressure plasma in the Earth's
382 magnetosphere, Annales Geophysicae, 22, 267-287, 2004.
383 Liu, J., Angelopoulos, V., Runov, A., and Zhou, X.-Z.: On the current sheets surrounding
384 dipolarizing flux bundles in the magnetotail: The case for wedgelets, J.Geophys.Res.,
385 118, 2000-20120, doi:10.1002/jgra50092, 2013.
386 Liu, J., Angelopoulos, V., Zhou, X.-Z., Yao, Z.-H., and Runov, A.: Cross-tail expansion of
387 dipolarizing flux bundles, J.Geophys.Res., 120, 2516-2530,
388 doi:10.1002/2015JA020997, 2015.
389 Lui, A.T.Y.: Current disruption in the Earth's magnetosphere: Observations and models, J.
390 Geophys. Res., 101, 13067-13088, 1996.
391 Machida, S., Miyashita, Y., Ieda, A., Nose, M., Nagata, D., Liou, K., Obara, T., Nishida, A.,
392 Saito, Y., and Mukai, T.: Statistical visualization of the Earth's magnetotail based on
393 Geotail data and the implied substorm model, Ann. Geophys., 27, 1035-1046, 2009.
394 Machida, S., Miyashita, Y., Ieda, A., Nose, M., Angelopoulos, V., and McFadden, J.P.:
395 Statistical visualization of the Earth's magnetotail and the implied mechanism of
396 substorm triggering based on superposed-epoch analysis of THMIS data, Ann.
397 Geophys., 32, 99-111, 2014.
398 McPherron, R.L., Russell, C.T., and Aubry, M.P.: Satellite studies of magnetospheric
399 substorms on August 15, 1968: 9. Phenomenological model for substorms, J.
400 Geophys. Res., 78, 3131-3148, 1973.
401 Miyashita, Y., Machida, S., Kamide, Y., Nagata, D., Liou, K., Fujimoto, M., Ieda, A., Saito,

M.H., Russell, C.T., Christon, S.P., Nose, M., Frey, H.U., Shinohara, I., Muaki, T., Saito, Y., and Hayakawa, H.: A state-of-the-art picture of substorm-associated evolution of the near-Earth magnetotail obtained from superposed epoch analysis, J. Geophys. Res., 114, A01211, doi:10.1029/2008JA013225, 2009.

Morioka, A., Miyoshi, Y., Miyashita, Kasaba, Y., Misawa, H., Tsuchiya, F., Kataoka, R., Kadokura, A., Mukai, T., Yumoto, K., Menietti, D.J., Parks, G., Liou, K., Honary, and Donovan, E.: Two-step evolution of auroral acceleration at substorm onset, J. Geophys. Res., 115, A11213, doi:10.1029/2010JA015361, 2010.

Nagai, T., Fujimoto, M., Saito, Y., Machida, S., Terasawa, T., Nakamura, R., Yamamoto, T., Mukai, T., Nishida, A., and Kokubun, S.: Structure and dynamics of magnetic reconnection for substorm onsets with Geotail observations, J. Geophys. Res., 103, A3, 4419-4440, 1998.

Nakamura, R., Baumjohann, W., Brittnacher, M., Sergeev, V.A., Kubyshkina, Mukai, T., and Liou, K.: Flow bursts and auroral activations: Onset timing and foot point location, J. Geophys. Res., 106, A6, 10777-10789, 2001.

Oguti, T., Kitamura, T., and Watanabe, T.: Global aurora dynamics campaign, 1985-1986, J. Geomag. Geoelectr, 40, 485-504, 1988.

Ohtani, S.-I., Miura, A., and Tamao, T.: Coupling between Alfven and slow magnetosonic waves in an inhomogeneous finite-β plasma: 1 Coupled equations and physical mechanism, Planet. Space Sci., 37, 567-577, 1989.

Ohtani, S.-I., and Tamao, T.: Does the ballooning instability trigger substorms in the near-earth magnetotail?, J. Geophys. Res., 98, A11, 19369-19379, 1993.

Rubtsov, A.V., Mager, P.N., and Klimushkin, D.Yu.: Ballooning instability of azimuthally small scale coupled Alfven and slow magnetoacoustic modes in two-dimensionally inhomogeneous magnetospheric plasma, Physics of Plasmas 25, 102903, doi:10.1063/1.5051474, 2018.

Runov, A., Angelopoulos, V., Zhou, X.-Z., Zhang, X.-J., Li, S., Plaschke, F., and Bonnell, J.: A THEMIS multicase study of dipolarization fronts in the magnetotail plasma sheet, 116, A05216, doi:10.1029/2010JA016316, 2011.

Saka, O., Akaki, H., and Baker, D.N.: A satellite magnetometer observation of dusk-to-dawn current in the midnight magnetosphere at low-latitude Pi2 onset, Earth Planets Space, 54, e1-e4, 2002

Saka, O., Hayashi, K, and Thomsen, M.: First 10 min intervals of Pi2 onset at geosynchronous altitudes during the expansion of energetic ion regions in the nighttime sector, J. Atmos. Solar Terr. Phys., 72, 1100-1109, 2010.

Saka, O., Hayashi, K., and Koga, D.: Excitation of the third harmonic mode in meridian planes

for Pi2 in the auroral zone, J. Geophys. Res., 117, A12215, doi:10.1029/2012JA018003, 2012.

Saka, O., and Hayashi, K.: Longitudinal expansion of field line dipolarization, J. Atmos. Solar Terr. Phys., 164, 235-242, 2017.

Saka, O.: A new scenario applying traffic flow analogy to poleward expansion of auroras, Ann. Geophys., 37, 381-387, 2019.

Sakurai, T., and Saito, T.: Magnetic pulsation Pi2 and substorm onset, Planet. Space Sci., 24, 573-575, 1972.

Takahashi, K., Anderson, B.J., and Ohtani, S.-I.: Multisatllite study of nightside transient toroidal waves, J.Geophys.Res., 101, A11, 24815-24825, 1996.

Yao, Z, Sun, W.J., Fu, S.Y., Pu, Z.Y., Liu, J., Angelopoulos, V., Zhang, X.-J., Chu, X.N., Shi, Q.Q., Guo, R.L., and Zong, Q.-G.:Current structures associated with dipolarization fronts, J.Geophys.Res., 118, 6980-6985, doi:10.1002/2013JA019290, 2013.

Figure captions

Figure 1.

A progress of field line thinning in the growth phase is illustrated. The inflow flux ($F_{\perp}$) rotated counterclockwise, from red, green, and to blue arrows in time. The rotation of the inflow vectors produced the field-aligned component of the flux, $\delta F_{//} = F_{\perp}(\omega \cdot \delta t)$ as depicted in the inset. Note that inflows are localized earthward of the outer field lines.

Figure 2.

Schematic illustration of the flux tube deformations associated with the slow magnetoacoustic wave. Parallel displacement, ξ_z, along the field lines and perpendicular displacement, $\xi_{\perp}$,

in longitude away from the center are coupled in the slow magnetoacoustic wave (see text for the explanation of equations (3) and (4)).

Figure 3.

A schematic illustration of the field line deformations in the meridian plane associated with the changing curvature radius of the field lines. The outer field lines marked by (1) changed to field lines (2) by increasing its curvature radius to R1 (red-dashed circle) in association with the onset of slow magnetoacoustic wave, while the inner field lines marked by (3) moved to field lines (4) of smaller curvature radius R2 (blue-dashed circle). This transition, (3) to (4), may be caused by the radial gradient of magnetic pressures becoming steeper in association with the inward compression of the field lines (see text).

Figure 4.

(A) Vertical component of $(rot\ \mathbf{J})_Z$ in the meridian chain along 300°E for the interval from 1000 UT to 1500 UT, reproduced from Saka and Hayashi (2017). Dipolarization onset was at 12:13 UT at this meridian. For the calculation of $(rot\ \mathbf{J})_Z$, vertical component data from RES (83.0°N), CBB (76.6°N), CONT (72.6°N), YKC (68.9°N), FSIM (67.2°N), FSJ (61.9°N), and VIC (54.1°N) were used (see text). Positive for the clockwise rotation (CW) of ionospheric currents and negative for the counterclockwise rotation (CCW) viewed from above the ionosphere. Amplitudes are color-coded. The scale is shown on the right. Demarcation lines separating CCW and CW in latitudes are marked by dashed line. The demarcation line moved to poleward after the onset. Note that negative $(rot\ \mathbf{J})_Z$ in poleward edge indicates smooth decrease of the Z amplitudes.

(B) Time progresses of the CW/CCW patterns are illustrated separately in five segments from 1 to 5 marked in Figure 4 (A). The figure demonstrates a progress of CW/CCW pair in time, CW in the poleward and CCW in the equatorward. This pair developed its size after onset showing poleward expansion. The meridional current associated with this pair of loop current, if closed in the equatorial plane via the field-aligned currents, comprised the Bostrom type current system.

Figure 5

(A) Difference of duskward flux (counts/sample) ($\mathbf{J}_-$) and dawnward flux ($\mathbf{J}_+$) from

1430 UT to 1600 UT, 31 August 1986 for 63-85 keV ion channel measured by AMPTE CCE spacecraft, reproduced from [Saka et al., 2002].

(B) Same as for (A) but for 125-210 keV ion channel. The satellite passed the midnight sector (20 – 23 MLT) from 3 Re to 7 Re at latitudes south of the equatorial plane (-8^{o} MLaT). Radial distance (R) in Re, MLaT in degree, and MLT at 15:00 UT and 16:00 UT along satellite trajectory are shown in the bottom.

(C) Multiple Pi2 event with positive bay observed at low latitude station (KUJ) at L=1.2 in the midnight sector. MLT of KUJ was 23:42 at 15:00 UT. Enhancement of the flux difference ($\mathbf{J}_{-} - \mathbf{J}_{+}$) occurred associated with the second onset of the positive bay marked by vertical arrow.
In the inset at right hand corner, radial profile of the ion flux was illustrated. Duskward flux represented by ($\mathbf{J}_{-}$) came from R_1 (earthward) and dawnward flux ($\mathbf{J}_{+}$) from R_2 (tailward). $\mathbf{J}_{-} > \mathbf{J}_{+}$ because of the pressure gradient positive earthward. Spatial gradient represented by solid line relaxed to dotted line by the Ballooning instability. Radial separation, $R_2 - R_1$, is either 1000 km or 1800 km for 63-85 keV ions or 125-210 keV ions, respectively. Spatial inhomogeneities of 125-210 keV ions relax faster than those of 63-85 keV ions.

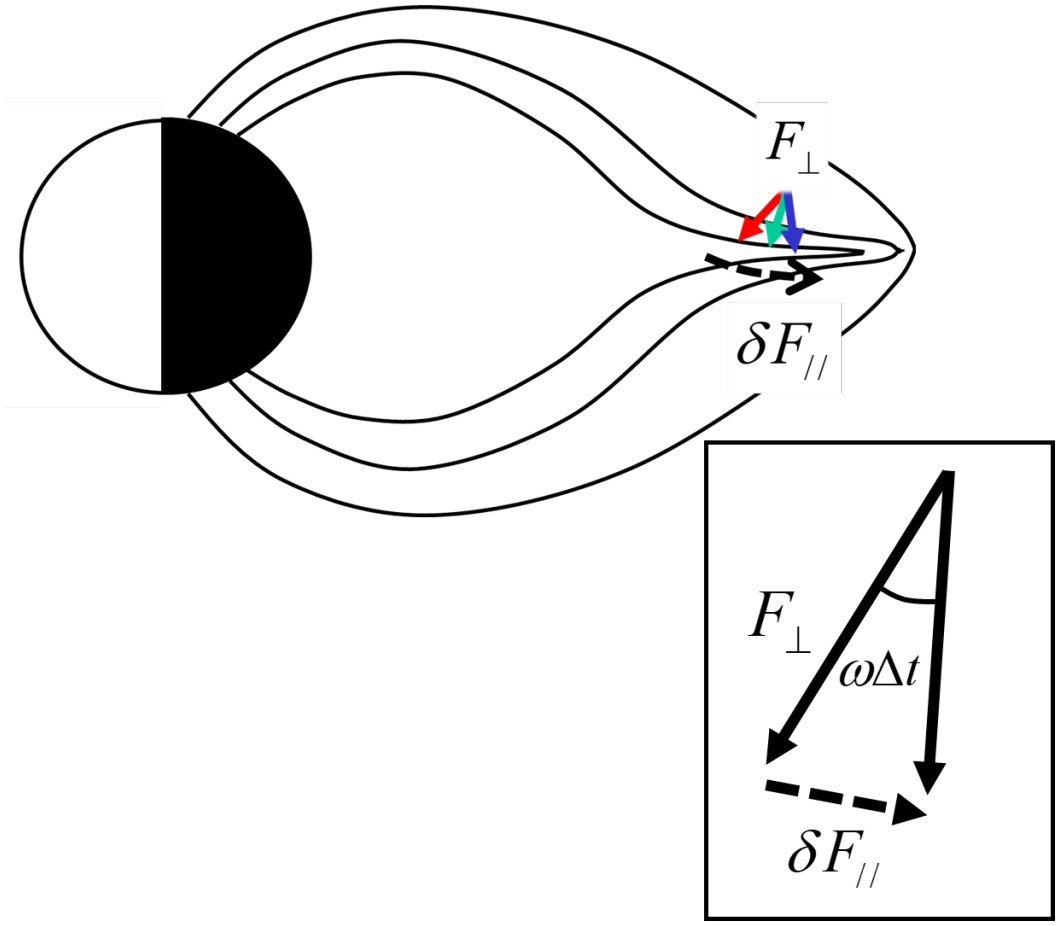

Figure 1

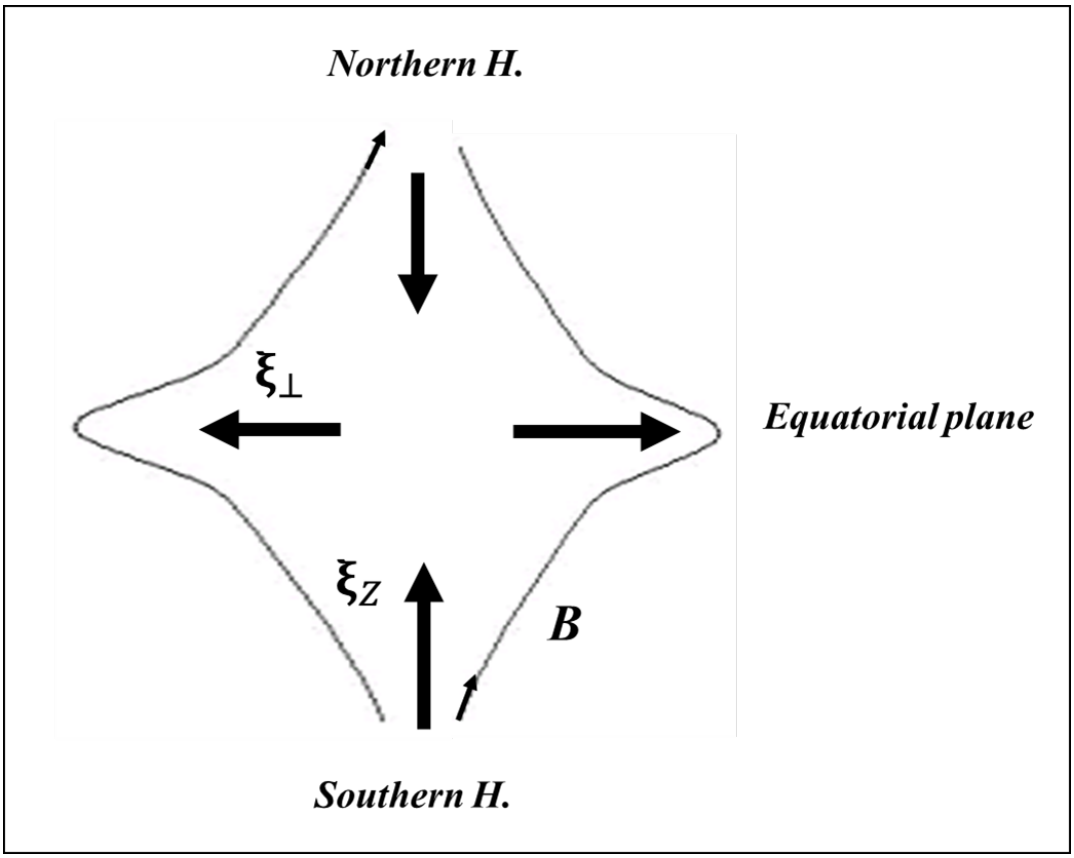

Figure 2

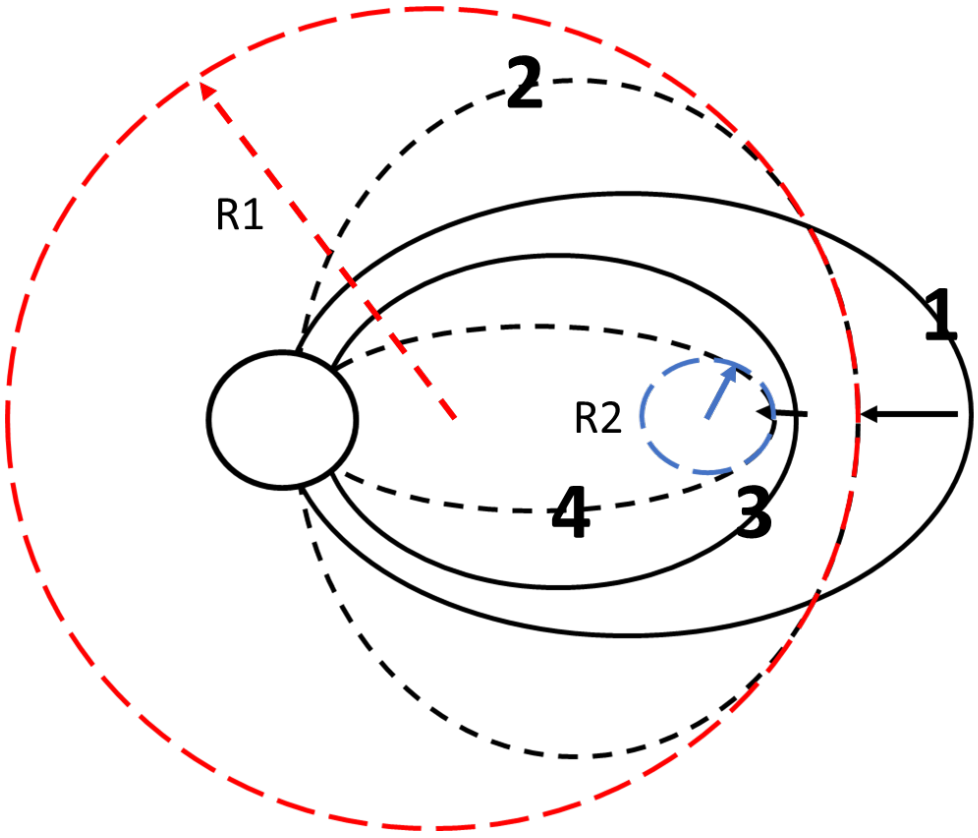

Figure 3

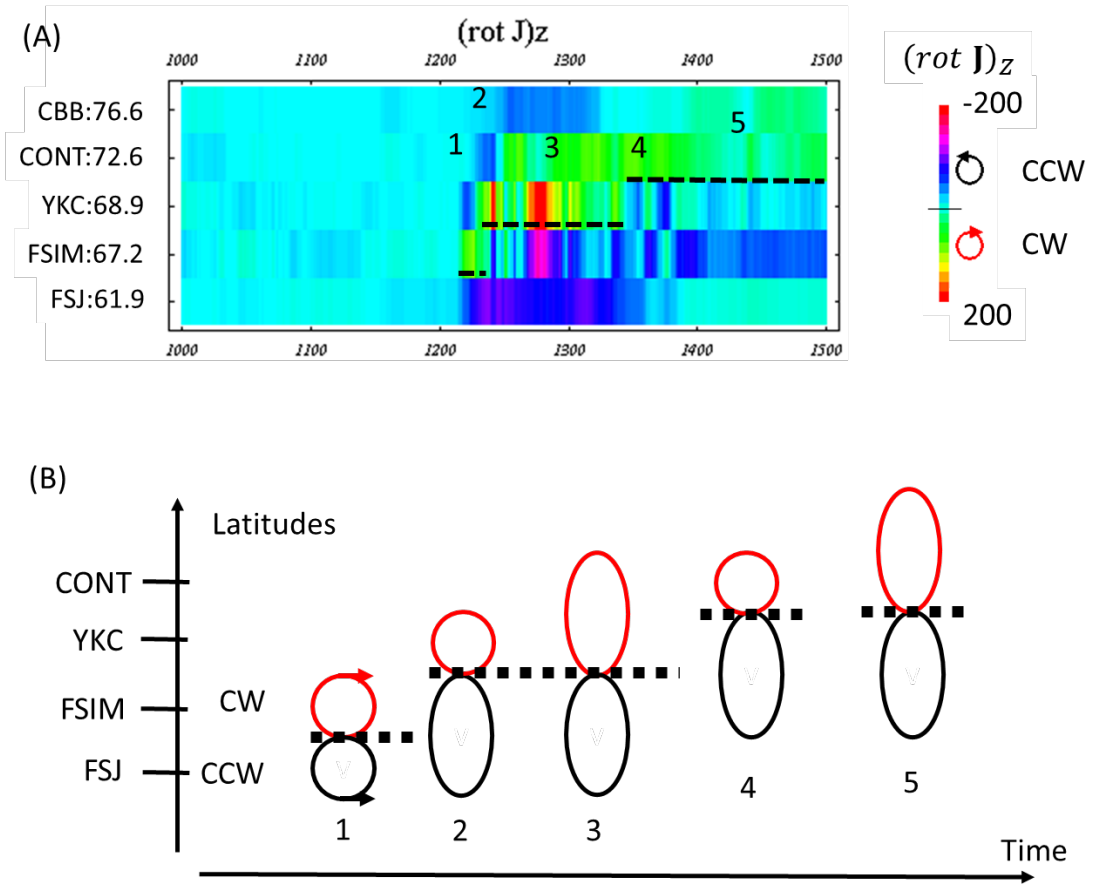
(A)
(rot J)z
1000
1100
1200
1300
1400
1500
CBB:76.6
CONT:72.6
YKC:68.9
FSIM:67.2
FSJ:61.9
1
2
3
4
5
$(rot\ \mathbf{J})_Z$
-200
CCW
CW
200
(B)
Latitudes
CONT
YKC
FSIM
FSJ
CW
CCW
1
2
3
4
5
Time

Figure 4

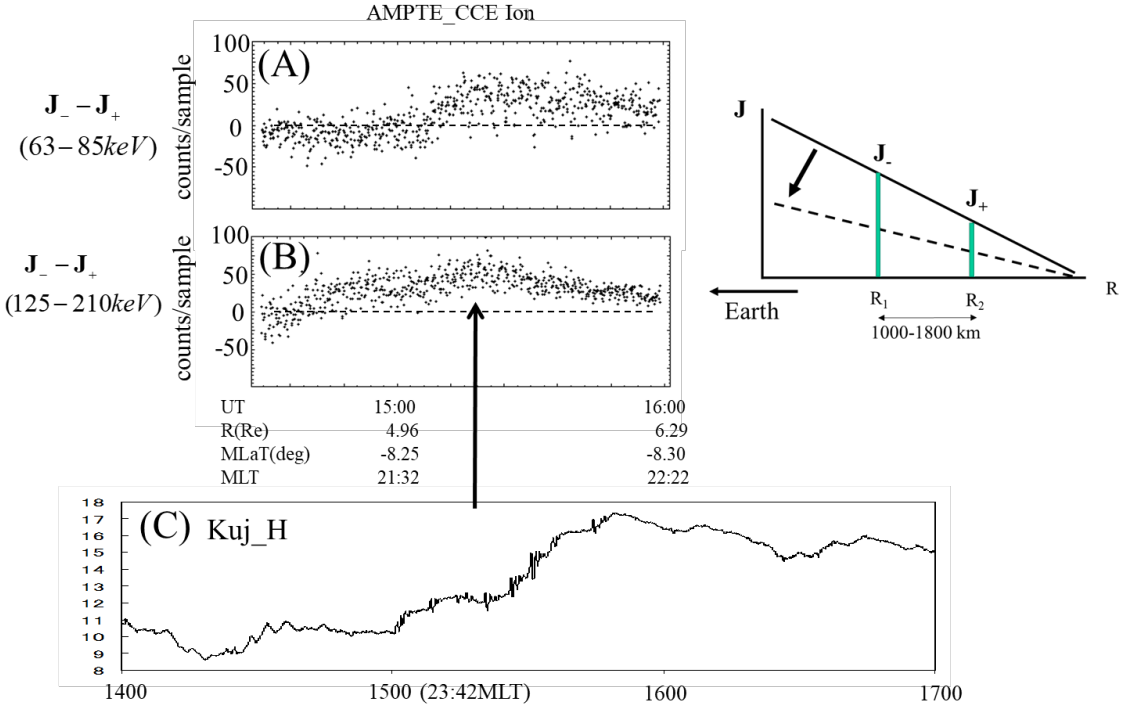
AMPTE_CCE Ion
$J_- - J_+$
$(63-85keV)$
counts/sample
100
50
0
-50
(A)
$J_- - J_+$
$(125-210keV)$
counts/sample
100
50
0
-50
(B)
UT 15:00 16:00
R(Re) 4.96 6.29
MLaT(deg) -8.25 -8.30
MLT 21:32 22:22
(C) Kuj_H
18
17
16
15
14
13
12
11
10
9
8
1400
1500 (23:42MLT)
1600
1700
J
J_-
J_+
R
Earth
R_1
R_2
1000-1800 km

Figure 5